

# Subspace Hybrid MVDR Beamforming for Augmented Hearing

Sina Hafezi, Alastair H. Moore, Pierre H. Guiraud, Patrick A. Naylor, *Fellow, IEEE*  
Jacob Donley, Vladimir Tourbabin, *Member, IEEE*, Thomas Lunner

**Abstract**—Signal-dependent beamformers are advantageous over signal-independent beamformers when the acoustic scenario - be it real-world or simulated - is straightforward in terms of the number of sound sources, the ambient sound field and their dynamics. However, in the context of augmented reality audio using head-worn microphone arrays, the acoustic scenarios encountered are often far from straightforward. The design of robust, high-performance, adaptive beamformers for such scenarios is an on-going challenge. This is due to the violation of the typically required assumptions on the noise field caused by, for example, rapid variations resulting from complex acoustic environments, and/or rotations of the listener’s head. This work proposes a multi-channel speech enhancement algorithm which utilises the adaptability of signal-dependent beamformers while still benefiting from the computational efficiency and robust performance of signal-independent super-directive beamformers. The algorithm has two stages. (i) The first stage is a hybrid beamformer based on a dictionary of weights corresponding to a set of noise field models. (ii) The second stage is a wide-band subspace post-filter to remove any artifacts resulting from (i). The algorithm is evaluated using both real-world recordings and simulations of a cocktail-party scenario. Noise suppression, intelligibility and speech quality results show a significant performance improvement by the proposed algorithm compared to the baseline super-directive beamformer. A data-driven implementation of the noise field dictionary is shown to provide more noise suppression, and similar speech intelligibility and quality, compared to a parametric dictionary.

**Index Terms**—Beamforming, speech enhancement, augmented reality, spatial filtering, microphone arrays, adaptive beamforming, MVDR, PCA

## I. INTRODUCTION

Colin Cherry was the first to identify the ‘cocktail party problem’ as the task of enhancing one target signal, or voice, in the presence of multiple interfering signals and noise [1, 2]. Despite advances in speech enhancement and microphone array processing, the cocktail party problem still remains a challenge in the audio signal processing community after decades of research [2, 3, 4]. Relevant applications include teleconferencing, speech recognition in human-machine interactions, hearing aids, and augmented reality audio.

It is widely known that significant enhancement can be achieved using the acoustic signals captured with a microphone array device [5, 6, 7, 8]. The use of wearable mi-

crophone arrays is a beguiling approach towards addressing the cocktail party problem. Wearable arrays, such as augmented reality (AR) glasses [3], can additionally provide head/array position and orientation information, as well as source directions of arrival (DOAs) and/or other environmental information obtained using a camera or other sensors. However, the compact size and real-world implementation of such systems restricts the processing to be computationally inexpensive, causal, real-time and robust to unforeseen scenarios. This paper addresses scenarios with one or more target talkers in the presence of localized interferers and ambient noise, using a head-worn microphone array mounted in AR glasses. It is assumed in the following that the array’s acoustic transfer functions (ATFs) and the target DOAs are known with realistic accuracy.

Multichannel speech enhancement systems [9] typically employ multiple-input single-output (MISO) algorithms exploiting spatial, temporal and spectral information to improve the signal-to-noise ratio (SNR) at the output. The potential for additional improvement using single-input single-output (SISO) post-processing, such as the Wiener filter [10], spectral subtraction [11] or deep learning (DL)-based methods [12, 13] is recognized but not studied here; the focus in this work is the MISO block in such systems. Without loss of generality, a multi-target scenario is considered as multiple single-target scenarios in which the same MISO method can be applied. Such decomposition of the scenario is known to improve the enhancement performance due to the use of fewer distortionless target constraints and correspondingly increase the potential for noise suppression. In addition, it enables control of the mixture of enhanced sources in the output depending on the application.

In this work, a novel analytical beamforming algorithm is proposed which is causal and able to adapt to complex and non-isotropic noise fields while being computationally efficient due to the use of pre-calculated weights. The dictionary of precalculated beamformer weights is shown to have the flexibility of being analytical (parametric) or data-driven. Early work on this topic was described in [14]. Here, the work has been extended to include a new formulation, the data-driven dictionary, more extensive evaluations and mathematical analysis of the method.

The remainder of the paper is structured as follows. Section II provides a brief review of beamforming approaches. Section III formulates the problem and defines the baseline beamformer. Sections IV and V respectively propose the multichannel enhancement system and two categories

S. Hafezi, A. H. Moore, P. Guiraud, and P. A. Naylor are with the Department of Electrical and Electronic Engineering, Imperial College London, UK (e-mail: {sina.hafezi, alastair.h.moore, p.guiraud, p.naylor}@imperial.ac.uk).

J. Donley, V. Tourbabin, and T. Lunner are with Meta Reality Labs Research, Redmond, Washington, USA (e-mail: {jdonley, vtourbabin, thlu}@meta.com).

This work was supported by Meta Reality Labs Research.

of parametric and data-driven dictionaries of beamformer weights. Section VI compares the two implementations of the proposed method with the baseline beamformer using real-world recordings and simulated cocktail party data with a head-worn microphone array. Finally, conclusions are given in Section VII.

## II. BACKGROUND REVIEW

Beamforming algorithms spatially filter a sound field with the aim of preserving signals from the target direction(s) while minimizing the power of all other signals in the output.

### A. Classical Beamforming Algorithms

The implementation of classical beamformers is characterized by a filter-and-sum structure, either in the time domain or short-time Fourier transform (STFT) domain, and is of relatively low computational complexity [15]. Signal-independent beamformers, such as delay-and-sum [16] and fixed versions of minimum variance distortionless response (MVDR) [17] use static, possibly switched, precalculated filter coefficients. On the other hand, adaptive beamformers such as MVDR or linearly constrained minimum variance (LCMV) [18] with dynamic covariance input can potentially improve performance by adapting their spatial filtering characteristics to a particular, and possibly time-varying, acoustic scenario. Such signal-dependent beamformers rely on the use of a signal covariance matrix (SCM) or noise covariance matrix (NCM), resulting in the minimum power distortionless response (MPDR)<sup>1</sup> [17, 19] or MVDR beamformers, respectively. The MVDR approach is often preferred due to real-world inaccuracies in the steering vector causing potential performance degradation in MPDR because of target signal cancellation [20, 21].

A common and robust choice for the NCM in MVDR implementations is a signal-independent model. Examples include the matched-filter beamformer [5, 22] in which the NCM is a multiple of the identity matrix, and the superdirective beamformer [23] in which the NCM is the covariance matrix corresponding to a spherically or cylindrically isotropic diffuse noise field. The use of a signal-dependent NCM potentially improves spatial filtering performance if it is estimated accurately. Some such adaptive beamformers aim to estimate NCM either directly during periods when the target signal is inactive, or indirectly by subtracting the target contribution from the SCM. Both these approaches require identification of time-frequency (TF) bins containing target signal activity using, for example, speech activity detection (SAD) or speech presence probability (SPP) methods [15].

In [24], the SCM is decomposed into isotropic, identity and plane-wave (PW) components followed by removal of any (near-) target PWs from the modelled SCM to avoid signal cancellation. Although some signal-dependent beamformers are shown [24] to perform better than signal-independent beamformers, such evaluations are typically limited to simulations or simple-scene real-recordings. These typically avoid

<sup>1</sup>We note that beamformer nomenclature varies and that the term MVDR is used by some authors for either or both of the MPDR and MVDR beamformers.

the real-world complexities of the cocktail party problem with wearable arrays such as rapid dynamics of the noise field due to head rotation or the presence of non-isotropic noise fields.

### B. Deep Learning Approaches

Typical DL-based MISO speech enhancement methods use neural networks to estimate either the output (end-to-end methods) [25], or other information such as the NCM or beamformer weights (‘neural beamforming’) [26]. In [27, 28, 29, 30], real- or complex-valued TF ratio masks are estimated while in [31, 32] the TF bins dominated by noise are identified to estimate the NCM for use in MVDR beamforming. The work in [33] employs a U-Net architecture to directly estimate complex-valued beamforming weights. An extension of this work using DCCRN [12] is also proposed in [34]. Similarly to other neural beamformers, FaSNet [35] aims to estimate the beamformer filters but in the time-domain using a temporal convolutional network. Although the evaluation results from some of these methods are exceptionally good, these systems are limited to offline and/or high-latency applications due to non-causality and relatively heavy computational load. Methods such as [33, 35] are causal and designed for low-latency purposes. However, so far, they have not been evaluated in real-world, unseen cocktail party scenarios. In addition, DL-based methods are typically trained for only a particular architecture, input format, sample rate, and array geometry. In order to handle extra inputs, such as head tracking information or changes in the above configurations, the models usually require re-training and, in some cases, re-designing.

## III. FORMULATION AND BASELINE BEAMFORMER

For notational simplicity, the formulation is provided for a single-channel output. However, the same procedure can be repeated assuming different reference channels for multi-channel output.

### A. Signals in the STFT domain

Let  $Y_q(\nu, \ell) \in \mathbb{C}$  denote the signal at microphone index  $q$ , frequency index  $\nu$  and time-frame index  $\ell$ . Using a PW representation, this can be expressed as

$$Y_q(\nu, \ell) = \sum_{j=1}^J X_{q,j}(\nu, \ell) + V_q(\nu, \ell), \quad (1)$$

where  $X_{q,j} \in \mathbb{C}$  and  $V_q \in \mathbb{C}$  are, respectively, the  $j$ -th plane-waves with unique DOAs, and the sensor noise at microphone  $q$ . For brevity, the  $(\nu, \ell)$  dependency will be omitted in the following when unambiguous.

Defining  $\mathbf{y} = [Y_1 \dots Y_Q]^T \in \mathbb{C}^{Q \times 1}$  as the vector of noisy microphone signals, the beamformer output is

$$Z = \mathbf{w}^H \mathbf{y}, \quad (2)$$

where  $\mathbf{w} \in \mathbb{C}^{Q \times 1}$  is the vector of beamformer weights and  $(\cdot)^H$  indicates Hermitian transpose.

## B. MVDR

In the MVDR beamformer design, the weights are given by [17]

$$\mathbf{w} = \frac{\mathbf{R}_\varepsilon^{-1} \mathbf{d}}{\mathbf{d}^H \mathbf{R}_\varepsilon^{-1} \mathbf{d}} \quad (3)$$

$$\text{with } \mathbf{R}_\varepsilon = \hat{\mathbf{R}}_{\mathcal{N}} + \varepsilon \mathbf{I} \quad (4)$$

$$\text{and } \varepsilon = \max \left( \frac{\lambda_{\max} - \kappa_0 \lambda_{\min}}{\kappa_0 - 1}, 0 \right), \quad (5)$$

where  $\mathbf{d} = \tilde{\mathbf{h}}(\Omega_s) \in \mathbb{C}^{Q \times 1}$  is the steering vector for the target DOA  $\Omega_s$ , and  $\tilde{\mathbf{h}}(\cdot)$  is the array's relative transfer function (RTF) that is determined as the array's ATF  $\mathbf{h}(\cdot)$  normalized by the reference output channel. The  $\hat{\mathbf{R}}_{\mathcal{N}} \in \mathbb{C}^{Q \times Q}$  is an estimate of the NCM,  $\mathbf{I} \in \mathbb{C}^{Q \times Q}$  is the identity matrix,  $\lambda_{\max}$  and  $\lambda_{\min}$  are the largest and smallest eigenvalues of  $\hat{\mathbf{R}}_{\mathcal{N}}$ , and  $\kappa_0$  is the maximum permitted condition number of  $\mathbf{R}_\varepsilon$  and, indirectly, constrains the norm of  $\mathbf{w}$  and the sensitivity of the beamformer to errors in  $\mathbf{d}$  [36, 37].

## C. Isotropic-MVDR (Superdirective) Beamformer

The baseline beamformer in this study is chosen to be the Isotropic-MVDR referred to as 'Iso' (also known as Maximum Directivity), in which a static, spherically diffuse sound field is assumed for the  $\hat{\mathbf{R}}_{\mathcal{N}}$  in (4). This is equivalent to assuming the presence of uncorrelated interference with equal power from all directions. The spherically isotropic diffuse covariance matrix can be obtained as

$$\mathbf{R}_\gamma = \int_{\Omega} \mathbf{h}(\Omega) \mathbf{h}^H(\Omega) d\Omega, \quad (6)$$

where  $\int_{\Omega} d\Omega = \int_0^{2\pi} \int_0^\pi \sin(\theta) d\theta d\varphi$  denotes integration along azimuth  $\varphi \in [0, 2\pi)$  and inclination  $\theta \in [0, \pi]$ .

In the case of using a discrete set of  $\Omega \in \mathcal{I}$  from a uniform grid of directions, (6) can be approximated by quadrature weighting giving

$$\mathbf{R}_{\text{Iso}} = \sum_{i \in \mathcal{I}} q_i \mathbf{h}(\Omega_i) \mathbf{h}^H(\Omega_i), \quad (7)$$

where  $q_i \in \mathbb{R}$  is the quadrature weight for each sample direction of  $\mathbf{h}$  given by [38] as

$$q_i = \frac{2 \sin \theta_i}{N_\varphi N_\theta} \sum_{p=0}^{\lceil 0.5 N_\theta - 1 \rceil} \frac{\sin((2p+1)\theta_i)}{2p+1}, \quad (8)$$

in which  $\theta_i$  is the inclination of sample point  $i$  and the number of sample points in azimuth and inclination are  $N_\varphi$  and  $N_\theta$  respectively.

Note that the quadrature weighting is done to preserve the uniform power isotropy by compensating for the higher density of points closer to the poles in a uniform grid spatial sampling scheme. The use of other spatial sampling schemes may require no or different weighting. Using  $\mathbf{R}_{\mathcal{N}} = \mathbf{R}_{\text{Iso}}$  in (4) and substituting into (2), the output of this beamformer is denoted as  $Z_{\text{Iso}}$ .

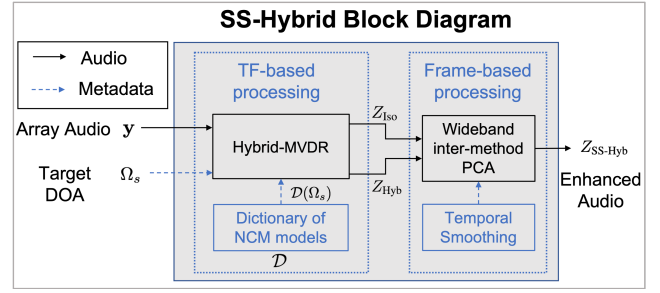


Fig. 1. The proposed system block diagram.

## IV. PROPOSED METHOD

As illustrated in Fig. 1, the proposed method consists of two stages. In the first stage (Hybrid-MVDR), multiple MVDR beamformers are implemented, each with a different precalculated  $\hat{\mathbf{R}}_{\mathcal{N}}$ , including isotropic and non-isotropic noise field models. The first stage outputs two signals:  $Z_{\text{Iso}}$  being the result of Iso and  $Z_{\text{Hyb}}$  being the output from the Hybrid-MVDR beamforming. The second stage applies wideband inter-method principal component analysis (PCA). This processes the two full-band spectral outputs from the first stage in order to remove the 'musical noise' generated in the output of the Hybrid-MVDR.

### A. Hybrid-MVDR

Multiple MVDR beamformers are implemented with the same steering vector but various NCMs taken from a dictionary of predefined and precalculated noise field models. The dictionary is denoted

$$\mathcal{D} = \{\mathbf{R}_{m,\nu} \rightarrow \mathbf{w}_{m,\nu,\Omega}\} \text{ for } \forall \nu \text{ and } \Omega \in \mathcal{I}_s \quad (9)$$

and contains the pre-calculated beamformer weights  $\mathbf{w}_{m,\nu,\Omega} \in \mathbb{C}^{Q \times 1}$ . The weights are derived using (3) for  $m = 1, \dots, M$  NCM models,  $\mathbf{R}_\varepsilon$ , and a discrete set  $\mathcal{I}_s$  of possible steering directions  $\Omega$ . Note that the dictionary  $\mathcal{D} \in \mathbb{C}^{M \times F \times Q \times \Psi}$  is a 4-dimensional table where  $M$ ,  $F$ ,  $Q$  and  $\Psi$  are respectively the total number of NCM models, frequency bands, microphones and steering directions.

The detailed choices of the NCM models in the dictionary  $\mathcal{D}$  will be discussed in Section V. For simplicity and as a necessity for the description of this section, it should be noted that the dictionary  $\mathcal{D}$  includes the isotropic model,  $\mathbf{R}_{\text{Iso}}$  in (7), as well as other models to be specified later.

At each TF bin  $(\nu, \ell)$ , and for a known steering direction  $\Omega_s(\ell)$ , the Hybrid-MVDR in Fig. 1 implements multiple MVDR beamformers using precalculated weights associated with the closest steering direction  $\Omega_s(\ell)$  stored in  $\mathcal{D}$ . The output with the minimum power among the models is selected and denoted as

$$Z_{\text{Hyb}} = (\mathbf{w}_j)^H \mathbf{y}, \quad (10)$$

$$\text{with } j = \arg \min_m \{ \|(\mathbf{w}_m)^H \mathbf{y}\|^2 \} \quad \forall \mathbf{w}_m \in \mathcal{D}(\Omega_s). \quad (11)$$

The isotropic model is included in  $\mathcal{D}$  and the corresponding beamformer  $Z_{\text{Iso}}$  is output to the next stage as shown in Fig. 1.

As will be shown in Section VI, although the Hybrid beamformer typically results in stronger acoustic noise reduction compared to Iso, the output may contain ‘musical noise’ due to rapid switching of beam pattern between neighbouring time-frames and frequencies. To suppress this musical noise, which is assumed to be sufficiently uncorrelated with the acoustic noise, the second stage extracts the component of the Hybrid-MVDR output which is correlated with the Iso-MVDR output.

### B. Wideband inter-method PCA

In this stage, a solution is proposed for the removal of the musical noise in the  $Z_{\text{Hyb}}$  while preserving its stronger noise suppression compared to  $Z_{\text{Iso}}$ . This section formulates the proposed solution whereas the Appendix provides a corresponding theoretical analysis.

Defining  $\check{(\cdot)}$  as the vector of full-band spectrum, let  $\check{\mathbf{z}}_{\text{Iso}}(\ell) = [Z_{\text{Iso}}(1, \ell), \dots, Z_{\text{Iso}}(F, \ell)] \in \mathbb{C}^{1 \times F}$  and  $\check{\mathbf{z}}_{\text{Hyb}}(\ell) = [Z_{\text{Hyb}}(1, \ell), \dots, Z_{\text{Hyb}}(F, \ell)] \in \mathbb{C}^{1 \times F}$  denote the full-band spectral outputs of Iso and Hybrid-MVDR beamformers at time-frame  $\ell$ , which are then concatenated to form a two-channel wideband data matrix  $\mathbf{Z} \in \mathbb{C}^{2 \times F}$  defined as

$$\mathbf{Z}(\ell) = \begin{bmatrix} \check{\mathbf{z}}_{\text{Hyb}}(\ell) \\ \check{\mathbf{z}}_{\text{Iso}}(\ell) \end{bmatrix}. \quad (12)$$

The inter-method wideband covariance matrix  $\mathbf{R}_z(\ell) \in \mathbb{C}^{2 \times 2}$  is then defined as

$$\mathbf{R}_z(\ell) = \mathbb{E}\{\mathbf{Z}(\ell)\mathbf{Z}(\ell)^H\}, \quad (13)$$

where  $\mathbb{E}\{\cdot\}$  is the expectation operator. An estimate of  $\mathbf{R}_z$  in (13) can be obtained by applying an exponential moving average (EMA) process to the instantaneous inter-method covariance matrix as

$$\hat{\mathbf{R}}_z(\ell) = \alpha \hat{\mathbf{R}}_z(\ell - 1) + (1 - \alpha)\mathbf{Z}(\ell)\mathbf{Z}(\ell)^H, \quad (14)$$

where  $0 < \alpha = e^{-\Delta t/T} < 1$  is the smoothing factor,  $\Delta t$  is the STFT time-frame step, and  $T$  is a forgetting time constant.

Using Eigenvalue Decomposition (EVD),

$$\hat{\mathbf{R}}_z(\ell) = \mathbf{U}(\ell)\mathbf{\Sigma}(\ell)\mathbf{U}^{-1}(\ell), \quad (15)$$

where  $\mathbf{U} \in \mathbb{C}^{2 \times 2}$  and  $\mathbf{\Sigma} \in \mathbb{R}^{2 \times 2}$  are, respectively, the eigenvectors and diagonal matrix of eigenvalues. Assuming the columns of  $\mathbf{\Sigma}$  are sorted in descending order of eigenvalues, the first column of  $\mathbf{U}(\ell) = [\mathbf{U}_S(\ell), \mathbf{U}_N(\ell)]$  is considered to be the signal eigenvector denoted as  $\mathbf{U}_S(\ell) \in \mathbb{C}^{2 \times 1}$ .

The Signal Subspace (SS) of the  $\mathbf{Z}(\ell)$  is reconstructed as

$$\mathbf{Z}_{\text{SS}}(\ell) = \mathbf{U}_S(\ell)\mathbf{U}_S^H(\ell)\mathbf{Z}(\ell), \quad (16)$$

where the first row of  $\mathbf{Z}_{\text{SS}}(\ell) = [\check{\mathbf{z}}_{\text{SS-Hyb}}(\ell)^T, \check{\mathbf{z}}_{\text{SS-Iso}}(\ell)^T]^T \in \mathbb{C}^{2 \times F}$  is the subspace-Hybrid (SS-Hybrid) output. In a compact form, the final output spectrum can be written in terms of weighted mixing of  $\check{\mathbf{z}}_{\text{Iso}}$  and  $\check{\mathbf{z}}_{\text{Hyb}}$  spectra as

$$\check{\mathbf{z}}_{\text{SS-Hyb}}(\ell) = \beta_{\text{Hyb}}(\ell)\check{\mathbf{z}}_{\text{Hyb}}(\ell) + \beta_{\text{Iso}}(\ell)\check{\mathbf{z}}_{\text{Iso}}(\ell), \quad (17)$$

$$\beta_{\text{Hyb}}(\ell) = U_1 U_1^*, \quad (18)$$

$$\beta_{\text{Iso}}(\ell) = U_1 U_2^*, \quad (19)$$

where the  $U_1$  and  $U_2$  are respectively the first and the second element in the subspace eigenvector  $\mathbf{U}_S(\ell) = [U_1, U_2]^T$  and  $(\cdot)^*$  denotes the complex conjugate. A mathematical analysis of  $\mathbf{Z}$  and  $\hat{\mathbf{R}}_z$  in terms of the target and residual noise from each beamformer is given in the Appendix.

## V. DICTIONARY

This section proposes two alternative dictionary designs  $\mathcal{D}$  for the Hybrid-MVDR: (A) Parametric or (B) Data-driven. The parametric dictionary consists of NCM models  $\mathbf{R}$  that are derived using array ATFs and a set of pre-defined noise field power distributions. The data-driven dictionary includes NCM models derived from a set of array recordings assuming the ground truth noise recordings are available. Details of these two categories are discussed next.

### A. Parametric Dictionary

A parametric dictionary can be formed by considering both spatially correlated and uncorrelated NCM models. An example of a spatially uncorrelated noise model is sensor noise that has no inter-channel correlation, whereas an example of a spatially correlated noise model is environmental noise with arbitrary isotropy.

It can be noted that, for spatially uncorrelated models, the NCM,  $\mathbf{R}$ , is directly formulated whereas for the spatially correlated models, the formulation is done for the noise field isotropy  $\mathcal{P}(\Omega)$ , which then can be used along with the available ATFs to obtain the NCM model  $\mathbf{R}$  as

$$\mathbf{R} = \sum_{i \in \mathcal{I}} \mathcal{P}(\Omega_i) q_i \mathbf{h}(\Omega_i) \mathbf{h}^H(\Omega_i). \quad (20)$$

1) *Identity (Spatially uncorrelated model)*: This model results in a diagonal NCM where the diagonal values represent the relative noise power at each sensor. Assuming a spatially and spectrally uniform (white) sensor noise power, this model is given as

$$\mathbf{R}_{\text{Identity}} = \mathbf{I}, \quad (21)$$

where  $\mathbf{I} \in \mathbb{C}^{Q \times Q}$  is the identity matrix. Note that the identity matrix can be replaced with a diagonal matrix with non-uniform values if the array sensors’ noise powers are available, non-uniform and spectrally non-white.

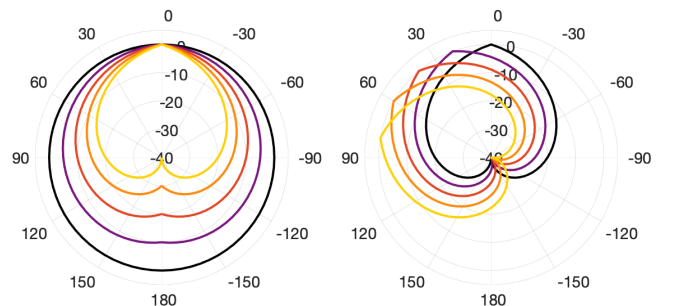


Fig. 2. (Left) Isotropic and horizontally unimodal Anisotropic models with a fixed  $\varphi_p = 0^\circ$  and varying  $\mathcal{A} = \{0, 10, 20, 30, 40\}$  dB. (Right) Anisotropic models with varying  $\varphi_p = \{0, 20, 40, 60, 80\}^\circ$  and fixed  $\mathcal{A} = 40$  dB.

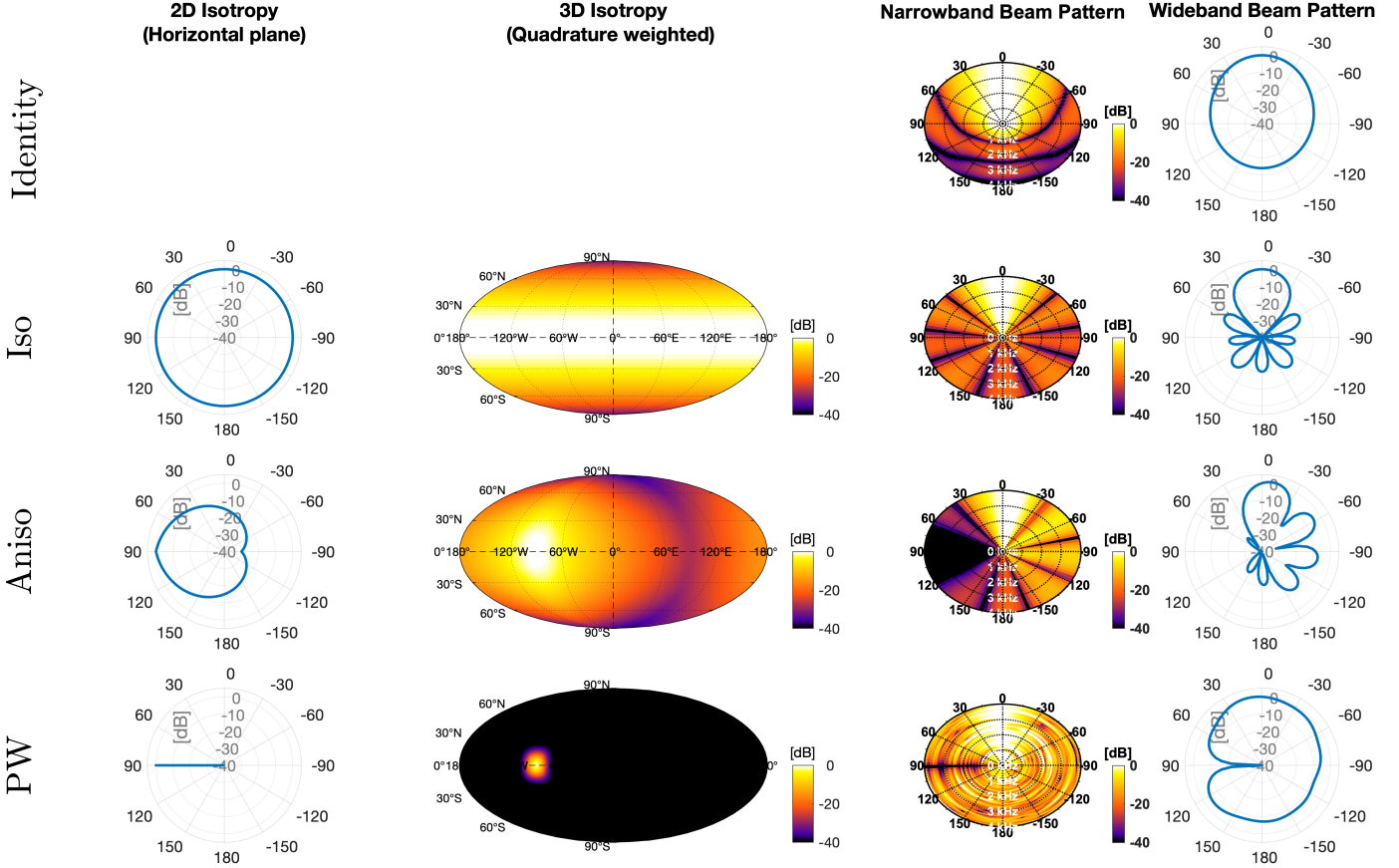


Fig. 3. Rows: Identity, Iso, unimodal Aniso and PW models with  $\varphi_p = 90^\circ$ . Columns: NCM 2D isotropy (horizontal plane), NCM 3D power distribution (quadrature weighted along the inclination), narrowband and wideband (a-weighted) beam patterns (horizontal plane) with steering direction  $\Omega_s = (\varphi_s, \theta_s) = (0, 90)^\circ$ .

2) *Isotropic model*: The spherically isotropic model has uniform isotropy across all directions and is given as

$$\mathcal{P}_{\text{Iso}}(\Omega) = 1. \quad (22)$$

Substituting (22) into (20) results in  $\mathbf{R}_{\text{Iso}}$ , which is equivalent to the  $\mathbf{R}$  used in (7) for the superdirective beamformer in Section III-C.

3) *Anisotropic models*: Anisotropic models can be defined in infinitely many ways. However, in this work, only horizontally unimodal (single-peak) isotropy is considered. Assuming a linear function for horizontal unimodality, the anisotropic model with a mode azimuth  $\varphi_p$  and power dynamic range  $\mathcal{A}$  (in decibels) is given as

$$\mathcal{P}_{\text{Aniso}}(\Omega) = 10^{-\mathcal{A}|\angle(\varphi, \varphi_p)|/(10\pi)}, \quad (23)$$

where  $\angle(\cdot, \cdot)$  is the angular difference in radians between two directions wrapped to  $[-\pi, \pi]$ . Note that the linearity of isotropy is on the logarithmic scale for the power, independent of the inclination  $\theta$  and symmetric around the mode azimuth  $\varphi_p$ . The  $\mathbf{R}_{\text{Aniso}}$  can be obtained by substituting (23) into (20). Figure 2 illustrates the horizontally unimodal anisotropic noise field models for a few examples with fixed  $\varphi_p$  and varying  $\mathcal{A}$  (left), as well as varying  $\varphi_p$  and fixed  $\mathcal{A}$  (right).

4) *Plane-wave models*: The PW model represents the effect of a single PW with DOA  $\Omega_p$  in matrix  $\mathbf{R}$ . This is formulated as

$$\mathcal{P}_{\text{PW}}(\Omega) = \begin{cases} 1 & \text{for } \Omega = \Omega_p \\ 0 & \text{otherwise} \end{cases}. \quad (24)$$

Empirical analysis suggested the removal of PW models from our implementations and evaluations. They were shown to be the most frequently chosen model in the Hybrid-MVDR. This commonly resulted in a failure to suppress the reverberation during target activity, due to the corresponding beam-pattern caused by the extreme directionality of PW model, as also shown in Fig. 3. An evaluation using PW models in the dictionary is presented in [14].

Figure 3 shows examples for the 1) Identity, 2) Iso, 3) unimodal Aniso and 4) PW models (with  $\varphi_p = 90^\circ$  for Aniso and PW) with their assumed 2D and 3D power distributions of NCM. Additionally shown are the resulting narrowband and wideband beam-patterns with steering direction  $\Omega_s = (\varphi_s, \theta_s) = (0, 90)^\circ$ . These results were obtained for a 32-element rigid spherical microphone array (SMA) with a radius of 4.2cm (corresponding to the em32 Eigenmike® [39]), with a sampling rate of 8 kHz and uniform spatial grid sampling of  $3^\circ$  resolution across both azimuth and inclination for the ATFs.

## B. Data-driven Dictionary

The data-driven dictionary contains NCM models estimated from noise-only array signals. The noise-only signals can be obtained either from signal segments during which the target is inactive, and/or exploiting ground truth noise signals if/when available. The term ‘ground truth noise signals’ refers to the array signal excluding the anechoic (direct-path) target. Hence, it includes the sensor noise, ambient and interferer(s) noise, as well as the target reverberation, since an ideal beamformer is expected to suppress the target reverberation as well as other sources of noise. Some ground truth noise signals are assumed to be available and can be obtained by simulating noisy scenarios using array’s ATFs.

Using EMA on the instantaneous ground truth covariance matrix, an estimate of the ground truth NCM can be derived as

$$\mathbf{R}_{\text{gt}}(\nu, \ell) = \alpha \mathbf{R}_{\text{gt}}(\nu, \ell - 1) + (1 - \alpha) (\mathbf{y}_{\text{gt}}(\nu, \ell) \mathbf{y}_{\text{gt}}^H(\nu, \ell)), \quad (25)$$

where  $\mathbf{y}_{\text{gt}} = \mathbf{y} - \mathbf{y}_{\text{target}}$  and  $\mathbf{y}_{\text{target}} \in \mathbb{C}^{Q \times 1}$  is the vector of anechoic target signals at the array sensors.

The number of the models  $M$  has no upper bound, unlike the number of channels  $Q$ , frequency bands  $F$  and the steering directions  $\Psi$  that are either defined in a wrapped space or imposed by the choice of the array and the STFT settings. In order to restrict the number of models  $M$  without imposing any restriction on the number of ground truth NCM observations, the set of measured  $\mathbf{R}_{\text{gt}}$  are compressed into a fixed number of bases  $\bar{\mathbf{R}}$  via k-means clustering, as next described.

1) *Vectorization of NCM*: Since k-means clustering operates on real-valued data, the complex-valued NCM matrix must be vectorized into real-valued vectors. The NCM matrix  $\mathbf{R} \in \mathbb{C}^{Q \times Q}$  has symmetric real values and conjugate complex values around its diagonal. In addition, the diagonal values are always real. This structure is utilized to form an efficient mapping between complex-valued matrix form denoted as  $\mathbf{R} \in \mathbb{C}^{Q \times Q}$  and real-valued vector form denoted as  $\mathbf{r} \in \mathbb{R}^{Q^2 \times 1}$  for NCM.

Figure 4 shows the process of conversion between the complex-valued matrix and real-valued vector forms. The complex-valued matrix  $\mathbf{R}$  is split into real and imaginary parts followed by the concatenation of  $Q^2$  unique real values from both real and imaginary matrices into one real-valued vector  $\mathbf{r}$ . This process is perfectly reversible.

2) *Clustering*: Having converted the arbitrary-size ( $N$ ) set of estimated ground truth NCMs  $\mathfrak{R}_\nu = \{\mathbf{R}_{\text{gt}}(\nu, \ell)\} \in \mathbb{C}^{N \times Q \times Q}$  per frequency band  $\nu$  into its vectorized form  $\mathbf{r}_\nu = \{\mathbf{r}_{\text{gt}}(\nu, \ell)\} \in \mathbb{R}^{N \times Q^2}$ , k-means is then used to cluster  $\mathbf{r}_\nu \in \mathbb{R}^{N \times Q^2}$  into  $\bar{\mathbf{r}}_\nu = \{\bar{\mathbf{r}}_{\text{gt}}(\nu, m)\} \in \mathbb{R}^{M \times Q^2}$  centroids, where the number of clusters  $K = M$  is set to the total number of models  $M$  in the dictionary. The real-valued vectorized basis NCM models are then converted into complex-valued matrix basis NCMs  $\bar{\mathfrak{R}}_\nu = \{\bar{\mathbf{R}}_{\text{gt}}(\nu, m)\} \in \mathbb{C}^{M \times Q \times Q}$ , which can be used in (3) to form the data-driven dictionary of beamformer weights.

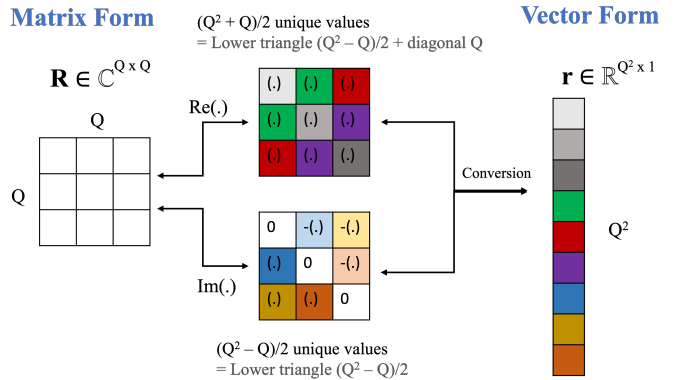


Fig. 4. The process of conversion between complex-valued matrix form  $\mathbf{R}$  and real-valued vector form  $\mathbf{r}$  of NCM.

Note that the use of k-means clustering results in the number of models being independent of the training set size  $N$ . This enables the use of a compact dictionary with relatively small  $M$  for computational efficiency, while benefiting from training on a large set of signals with relatively large  $N$ .

## VI. EVALUATIONS

The algorithm was evaluated in the context of augmented hearing and augmented reality audio. Two implementations of the proposed method with parametric and data-driven dictionaries were compared with the Iso-MVDR baseline beamformer, as well as the ‘passthrough’ signal at the reference microphone. Data was obtained using a head-worn microphone array in real-recordings, and from simulated ‘cocktail party’ scenarios.

### A. Head-worn microphone array

The head-worn ‘glasses’ microphone array from EasyCom dataset [3] was used. As shown in Fig. 5, it is a 6-channel array with four microphones on the glasses and two in-ear microphones. The ATFs were measured for a quasi-uniform grid of directions with coverage range of  $[-174^\circ, 180^\circ]$  and  $[-66^\circ, 84^\circ]$  and resolution of  $6^\circ$  and  $9^\circ$  across azimuth and elevation, respectively. The measurement was done using a manikin head wearing the array in an anechoic chamber of Meta Reality Labs.



Fig. 5. Head-worn ‘glasses’ microphone array used in EasyCom [3]. Microphones 5 and 6 are in-ear microphones.

## B. Dataset

The evaluation was performed using part of the SPEECH Enhancement for Augmented Reality (SPEAR) dataset [4], which is an extension of the EasyCom dataset [3]. The EasyCom dataset contains several realizations of a scenario illustrated in Fig. 6 in which a small group of people, sitting around a table in a room, have a natural conversation surrounded by ten loudspeakers playing restaurant-like ambient noise. The SPEAR dataset is split into sub-datasets where the first, D1, is the entire real-recording EasyCom dataset, and the second, D2, contains the simulated version of EasyCom (D1).

In EasyCom (D1), one participant (ID=2) was wearing the array while others were only wearing a close-talking headset microphone used as an approximate reference signal. Although a variety of metadata is provided in EasyCom, the tested beamformers only used the array’s ATFs, the target DOAs relative to the wearer (ID=2) and head-tracking data for each talker obtained from an optical motion capture system. The talkers’ close-talking headset microphone was only used as the reference signal during calculation of intrusive metrics in D1.

The D1 dataset embodies real-world realism and complexity. However, in such recordings, it is impossible to define the ground truth signals (direct-path target) at the array, that are normally required as reference signals for the calculation of instrumental (objective) intrusive metrics. Although close-talking headset microphone recordings for each talker are provided in EasyCom, their use in calculation of intrusive evaluation metrics would introduce reference signal errors. Such errors may be caused by, for example, sensor noise, cross-talk leakage from other talkers, the frequency response of the close-talking microphone and its position relative to the mouth, as well as the potential inaccuracy in time and level alignments. Hence, our evaluation also uses the D2 simulated dataset where the true reference signals (noise-free direct-path target at the array) are available, at the cost of degraded realism compared to D1. The access to the ground truth noise signals for the data-driven dictionary is also important and only available in D2.

In terms of the scenarios, both D1 and D2 share the same room dimensions of approximately  $7 \times 6 \times 3$  m, reverberation

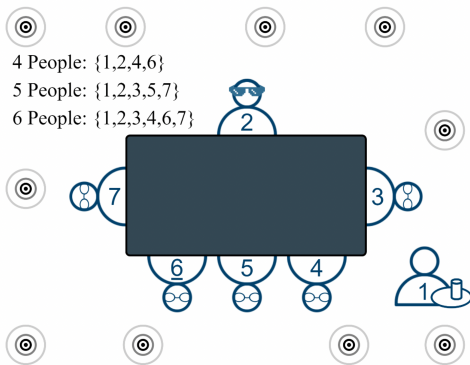


Fig. 6. Schematic of the scene used in EasyCom [3]. The ‘waiter’, ID=1, is not wearing a close-talking microphone and their position is not tracked.

time  $RT_{60} = 645$  ms and ten fixed loudspeakers distributed across the room playing uncorrelated, restaurant-like ambient noise. The D2 dataset was simulated using the TASCAR software platform [40] with the presence of a table and the walls of approximate dimensions. The talkers’ source signals in D2 were the D1 talkers’ close-talking headset microphone signals, denoised using the CEDAR DNS Two plugin. Unlike D1 where the ATFs can slightly vary due to different persons wearing the array, the simulations in D2 were based on the same measured ATFs provided in [3]. The D2 dataset also used the same head-tracking data and voice activity labels as provided in EasyCom.

In order to evaluate the effect of noise suppression on the localized interferer(s) such as the interfering talkers, the scenarios in EasyCom are divided into 6 s segments such that the following conditions are met:

- 1) Only one of the talkers is assumed as the target.
- 2) The target onset occurs after 2 s based on the voice activity metadata.
- 3) The wearer participant (ID=2) is not active.
- 4) The ‘waiter’ participant (ID=1) whose DOA and reference signal are unavailable is not the target.

The segments that do not meet these constraints are discarded. Note that while the selected segments share these constraints, they can still differ in talker, utterance, number of active sources and DOAs. For the visualization of these results, the selected segments were categorized according to the number of active sources per segment, denoted as  $N_s = [1, 2, 3]$ . The same segments from both D1 and D2 were used in the evaluation.

## C. Methods

The evaluation compares the proposed SS-Hybrid method, including parametric and data-driven dictionaries, denoted as ‘SSH’ and ‘SSH-K’, respectively, with the baseline superdirective beamformer denoted as ‘Iso’, and the passthrough signal at the reference channel denoted as ‘Pass’.

To avoid spatial aliasing due to the array geometry, data was lowpass filtered and down-sampled to 10 kHz sample rate. The STFT used a 16 ms time-window and 8 ms step. Microphone 2 (mid-front in Fig. 5) was selected as the reference channel. Empirical analysis showed that no condition number limiting on  $\mathbf{R}$  in (3) was needed for any of the beamformers and therefore  $\varepsilon = 0$  in (4). The steering vector at each time-frame was updated with the RTF associated with the closest direction to the target DOA from the set of ATF measurement points described in Section VI-A. The settings associated with each method were as follows.

1) *Iso (baseline superdirective)*: The directions set  $\mathcal{I}$  in (7) used all the available ATF measurement points described in Section VI-A with quadrature weighting as in (8).

2) *SSH (SS-Hybrid with parametric dictionary)*: The parametric dictionary contained an isotropic model  $\mathbf{R}_{\text{Iso}}$  as in Iso, an identity model  $\mathbf{R}_{\text{Identity}}$ , and 300 unimodal anisotropic models  $\mathbf{R}_{\text{Aniso}}$  as in (23) with all possible pairs between sixty different  $\varphi_p = \{0, 6, \dots, 354\}^\circ$  and five different  $\mathcal{A} = \{8, 16, 24, 32, 40\}$  dB. This results in total of  $M = 302$  models. The set of possible steering directions was limited to  $\pm 90^\circ$

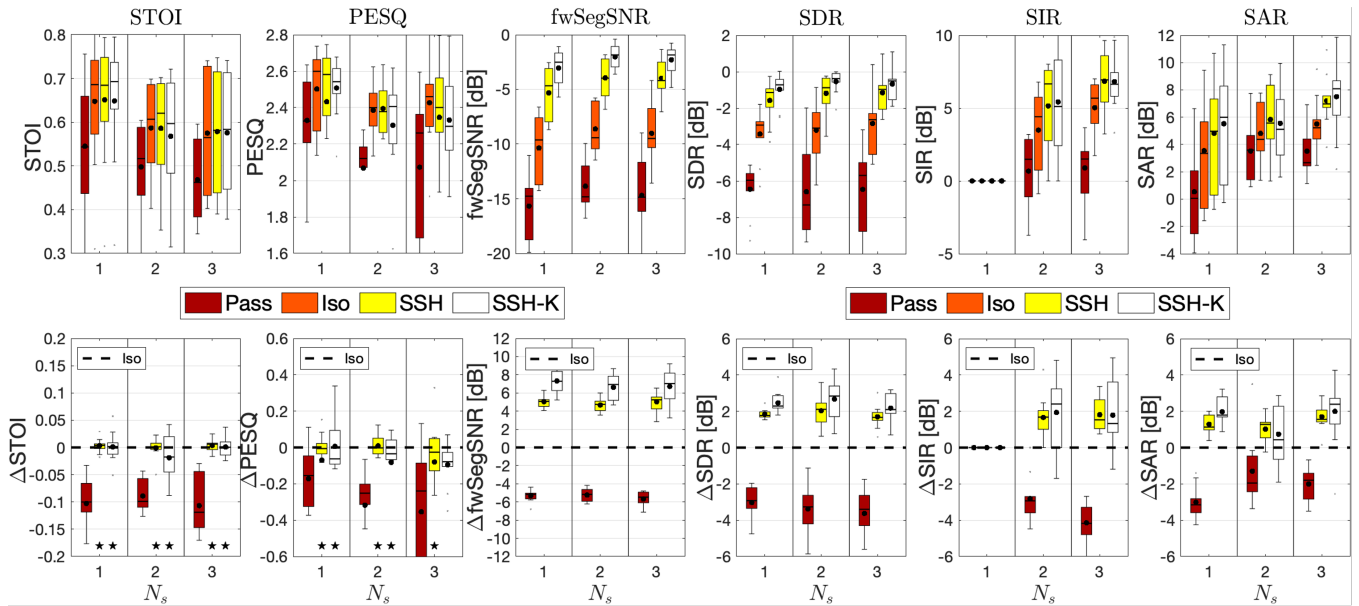


Fig. 7. The absolute (top row) and relative (bottom row) STOI, PESQ, fwSegSNR, SDR, SIR and SAR scores of methods for  $N_s = [1, 2, 3]$  in D1 dataset.

azimuth and  $\pm 30^\circ$  elevation resulting in total of  $\Psi = 217$  possible steering directions. Considering  $F = 81$  frequency bands based on the sample rate and the STFT settings as well as  $Q = 6$  channels based on the array configuration, the dictionary  $\mathcal{D}$  in (9) becomes a  $302 \times 81 \times 6 \times 217$  table containing approximately 32 million complex numbers. The time constant for the smoothness factor,  $\alpha$ , in (14) was empirically set to  $T = 80$  ms.

3) *SSH-K (SS-Hybrid with data-driven dictionary)*: Apart from the content of the dictionary, the settings for SSH-K were the same as for SSH unless stated otherwise. The set of ground truth NCM estimates  $\mathfrak{R}_\nu = \{\mathbf{R}_{\text{gt}}(\nu, \ell)\}$  in Section V-B2 were obtained using (25) on half of the segments with  $N_s = 1$  in D2, which resulted in approximately  $N = 7500$  time-frames. The segments included in the training set were excluded from the evaluation results. The k-means clustering had random centroid initialization and used  $K = M = 302$  in order to have the same number of models in both data-driven and parametric dictionaries. The Iso model was additionally added to the data-driven dictionary as a requirement in Hybrid-MVDR.

#### D. Metrics

The single-channel output of each method was compared with the reference signal for six intrusive metrics: short-time objective intelligibility measure (STOI) [41], perceptual evaluation of speech quality (PESQ) [42, 43], frequency-weighted segmental SNR (fwSegSNR) [44, 45], signal-to-distortion ratio (SDR) [46], signal-to-interference ratio (SIR) [46] and signal-to-artifact ratio (SAR) [46]. The VOICEBOX MATLAB toolbox [47] was used for STOI, PESQ and fwSegSNR while the PEASS MATLAB toolbox [48, 49] was used for the SDR, SIR and SAR.

These metrics evaluate the performance of speech enhancement in terms of speech intelligibility (STOI), speech quality (PESQ) and the noise suppression (fwSegSNR, SDR,

SIR, SAR). As for the reference signal used in the intrusive metric calculations, in the D1 dataset, the close-talking headset microphone signal was time- and level-aligned to the array ‘passthrough’ signal at the reference channel using `sigalign` function from the VOICEBOX toolbox [47]. The true reference signal (noise-free direct-path target) was available in the D2 dataset.

#### E. Results: Real-recordings (D1)

Figure 7 shows the distributions of the absolute (top row) and the relative (bottom row) STOI, PESQ, fwSegSNR, SDR, SIR and SAR scores of the methods for varying  $N_s = [1, 2, 3]$  using the real-recording D1 dataset. The boxes show the upper and lower inter-quartile range with mean and median indicated by black dot ( $\bullet$ ) and horizontal dash (-) markers, respectively. The whiskers extend to 1.5 times of the inter-quartile range. In the bottom row plots, the presence of a star indicates no statistically significant difference from the baseline Iso beamformer (dashed line) according to paired t-test at  $p = 5\%$  level. The discussion of the results based on the category of metrics is as follows.

1) *D1 Speech Intelligibility (STOI)*: As shown in Fig. 7 first column, all beamformers improved the STOI compared to passthrough by a mean  $\Delta\text{STOI} = 0.1$ . Both SS-Hybrid implementations (SSH and SSH-K) preserved the same STOI improvement as the baseline Iso.

2) *D1 Speech Quality (PESQ)*: The second column of Fig. 7 also shows the same improvement in PESQ scores with mean  $\Delta\text{PESQ} = [0.2, 0.3, 0.4]$  for all beamformers compared to passthrough in  $N_s = [1, 2, 3]$  respectively, with an exception for SSH-K in  $N_s = 3$  with slightly less  $\Delta\text{PESQ}$  than Iso and SSH.

3) *D1 Noise Suppression (fwSegSNR, SDR, SIR, SAR)*: The third to the sixth columns in Fig. 7 show the suppression results for different definitions of noise. As expected,



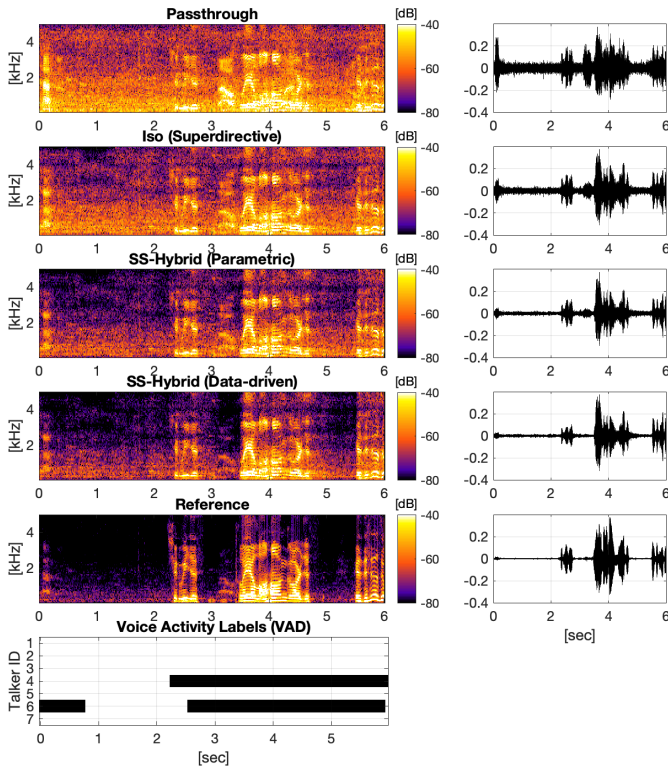


Fig. 8. The output spectrogram and waveform for each method from an example trial with  $N_s = 2$  in real-recording D1 dataset.

all beamformers significantly reduced the noise compared to the passthrough. Both versions of the proposed method significantly outperformed the baseline Iso by an average of 5 dB for fwSegSNR and 3 dB for SDR, SIR and SAR, in addition to the noise suppression achieved by Iso. The data-driven dictionary (SSH-K) suppressed noise 2 dB more than the parametric dictionary (SSH) due to the use of the data-driven NCMs.

Figure 8 illustrates the spectrogram and waveform outputs of Pass, Iso, SSH, SSH-K and the Reference signals from an example in D1 with an overlapping interferer talker ( $N_s = 2$ ). In line with the metrics discussed previously, it can be seen that the proposed SS-Hybrid method provides stronger noise suppression, while preserving the target signal as well as the baseline Iso. This example also shows the noise suppression superiority of data-driven (SSH-K) over parametric (SSH) dictionaries for the proposed method. Audio demo examples for this and other cases from both D1 and D2 datasets are available in [50].

4) *Musical Noise Removal*: As shown in the spectrograms of Iso, Hybrid and SS-Hybrid in Fig. 9, the musical noise in the Hybrid (middle row) is successfully removed by the inter-method wideband PCA in SS-Hybrid (bottom row) while preserving its extra noise suppression compared to Iso (top row).

#### F. Results: Simulation (D2)

Figure 10 shows the distributions of the absolute (top row) and the relative (bottom row) metrics for the methods for

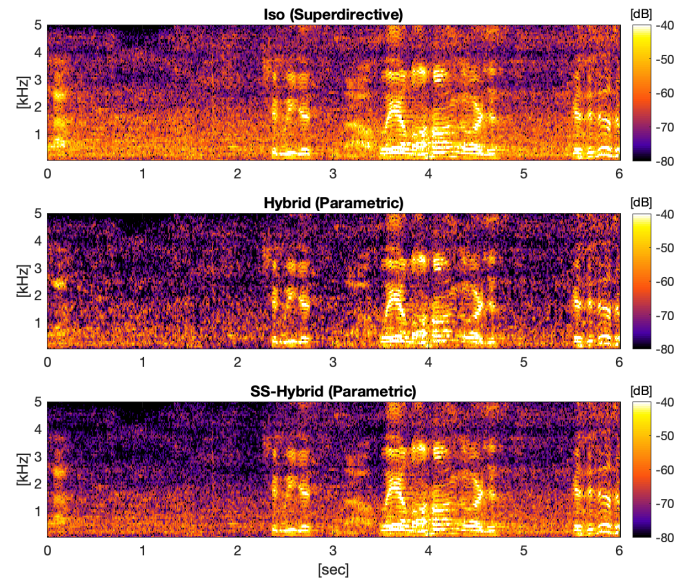


Fig. 9. The spectrogram outputs of Iso, Hybrid and SS-Hybrid for the same example as in Fig. 8.

varying  $N_s = [1, 2, 3]$  using the simulated D2 dataset. All beamformers improved all metrics compared to passthrough as expected.

1) *D2 Speech Intelligibility (STOI)*: Both variations of the proposed SS-Hybrid method (SSH and SSH-K) at least maintain the same intelligibility improvement as in the baseline Iso with the exception of data-driven SSH-K providing marginally higher  $\Delta$ STOI improvement for  $N_s = 2$ .

2) *D2 Speech Quality (PESQ)*: Similar to the STOI results, both SSH and SSH-K preserve the same PESQ improvement achieved by the baseline beamformer with an average  $\Delta$ PESQ = 0.3 for all beamformers compared to the passthrough.

3) *D2 Noise Suppression (fwSegSNR, SDR, SIR, SAR)*: As expected and similar to the D1 dataset, the two versions of the proposed method (SSH and SSH-K) significantly outperform the baseline Iso in all noise suppression metrics by an average of  $\Delta$ fwSegSNR = 6 dB and 3 dB for SDR, SIR and SAR. The SS-Hybrid with data-driven dictionary (SSH-K), compared to the parametric dictionary (SSH), provides mean improvements in noise suppression of 4 dB in fwSegSNR and 2 dB in SDR, SAR and SIR for the reasons discussed in Section VI-E3. The good performance of the proposed methods shows robustness to an increase in the number of active sources ( $N_s$ ) and is consistent between the real-recording (D1) and simulated (D2) datasets.

## VII. CONCLUSIONS

A method of beamforming is proposed for multi-channel speech enhancement that is adaptive and signal-dependent while being comparable in terms of computational cost to static and signal-independent beamformers. The proposed beamformer uses a dictionary of pre-calculated weights. The method operates in two stages where, in the first stage, multiple MVDR beamformers are implemented using a weight

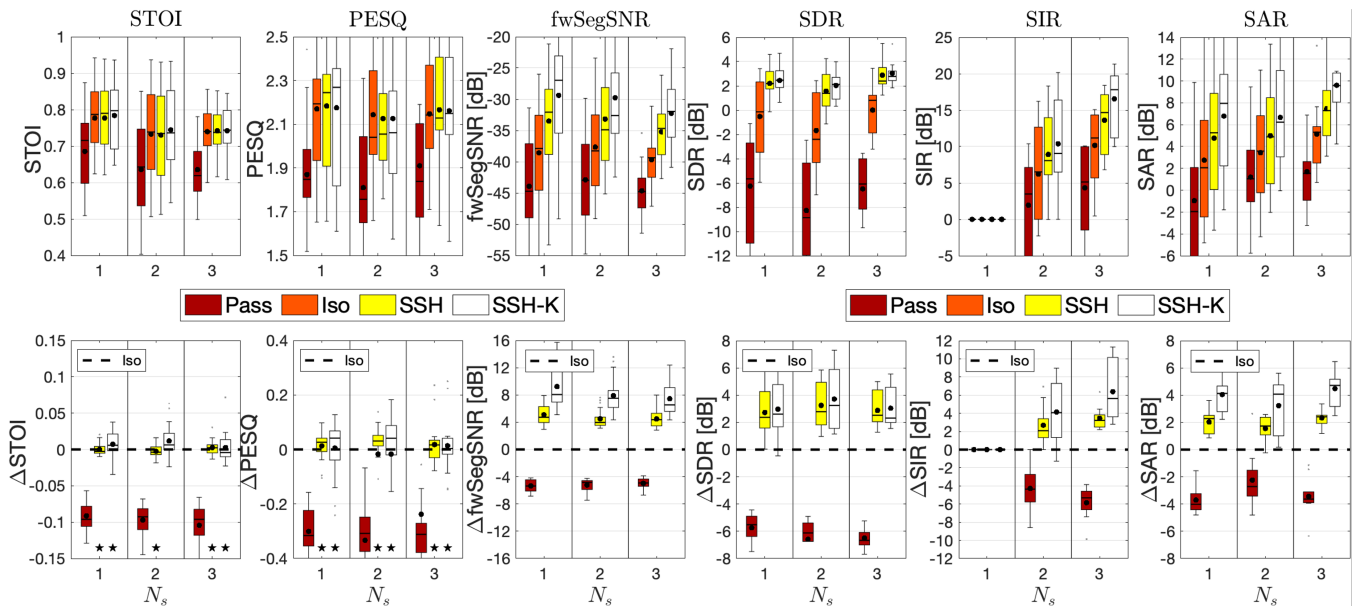


Fig. 10. The absolute (top row) and relative (bottom row) STOI, PESQ, fwSegSNR, SDR, SIR and SAR scores of methods for  $N_s = [1, 2, 3]$  in D2 dataset.

dictionary with entries corresponding to different noise covariance models. In the second stage, a wideband inter-method PCA is applied to the outputs of both static isotropic and adaptive Hybrid-model beamformers per time-frame to remove any ‘musical noise’ caused by the Hybrid MVDR beamforming. Two alternative dictionary designs were investigated: a parametric dictionary using isotropic and horizontally unimodal anisotropic noise field isotropy assumptions, and a data-driven dictionary using k-means clustering and ground truth-aware estimates of the noise covariance matrices from a simulated dataset. In the context of augmented hearing and augmented reality audio, evaluations were performed using real recordings of ‘cocktail party’ scenarios with approximate reference signals, and simulations with accurate reference signals for a 6-channel head-worn microphone array. The results for both real recordings and simulations showed significant performance benefits of the proposed method compared to the baseline superdirective beamformer. In terms of noise suppression, average improvements of 6 dB fwSegSNR and 3 dB SDR, SIR and SAR were found, while improvements in speech intelligibility (STOI) and quality (PESQ) were at least as good as the baseline superdirective beamformer. The use of a data-driven dictionary design, compared to the parametric dictionary, in the proposed method provided 1 to 2 dB more noise suppression with a corresponding improvement in the speech intelligibility and quality.

#### APPENDIX

The plane-wave representation of the array signal in (1) with  $J$  PWs can be re-written by separating the target PW and the remaining  $J - 1$  PWs as

$$Y_q(\nu, \ell) = S_q(\nu, \ell) + \sum_{j=1}^{J-1} X_{q,j}(\nu, \ell) + V_q(\nu, \ell), \quad (26)$$

where  $S_q = X_{q,j} \in \mathbb{C}$  is the  $j$ -th PW associated with the target direction  $\Omega_s$ . Since formulations for the remaining of this section will be all for a reference microphone, the microphone index  $q$  will be omitted for notational simplicity. Equation (26) can be written for the full-band spectrum at a reference microphone as

$$\tilde{y}(\ell) = \check{s}(\ell) + \check{\mathbf{x}}(\ell) + \check{\mathbf{v}}(\ell) \quad (27)$$

$$= \check{s}(\ell) + \check{\mathbf{n}}(\ell) \quad (28)$$

where  $\tilde{y} \in \mathbb{C}^{1 \times F}$ ,  $\check{s}$ ,  $\check{\mathbf{x}} = \sum_{j=1}^{J-1} \check{\mathbf{x}}_j$  and  $\check{\mathbf{v}}$  are the full-band spectrum of the array, target PW and the remaining PWs while  $\check{\mathbf{n}} = \check{\mathbf{x}} + \check{\mathbf{v}}$  denotes the residual noise spectrum including the mixture of non-Target PWs and the sensor noise.

The MVDR spectral output of Iso and Hybrid with steering direction  $\Omega_s$  can be written as

$$\check{\mathbf{z}}_{\text{Iso}}(\ell) = \check{s}(\ell) + \check{\mathbf{n}}_{\text{Iso}}(\ell), \quad (29)$$

$$\check{\mathbf{z}}_{\text{Hyb}}(\ell) = \check{s}(\ell) + \check{\mathbf{n}}_{\text{Hyb}}(\ell), \quad (30)$$

where  $\check{\mathbf{n}}_{\text{Iso}}$  and  $\check{\mathbf{n}}_{\text{Hyb}}$  are the residual noise in the output of Iso and Hybrid-MVDR beamformers assuming the target PW  $\check{s}$  is preserved due to the distortionless response constraint in the MVDR formulation. Note that  $\check{\mathbf{n}}_{\text{Iso}}$  and  $\check{\mathbf{n}}_{\text{Hyb}}$  are the frequency-dependent scaled versions of  $\check{\mathbf{n}}$  in (28) where the scaling coefficients are determined by the narrowband complex-valued beam patterns. The  $\check{s}$ ,  $\check{\mathbf{n}}_{\text{Iso}}$  and  $\check{\mathbf{n}}_{\text{Hyb}}$  are expected and assumed to be uncorrelated.

Substituting (29) and (30) in (12) gives

$$\mathbf{Z} = \begin{bmatrix} \check{\mathbf{s}} \\ \check{\mathbf{s}} \end{bmatrix} + \begin{bmatrix} \check{\mathbf{n}}_{\text{Hyb}} \\ \check{\mathbf{n}}_{\text{Iso}} \end{bmatrix}, \quad (31)$$

where time-frame dependency ( $\ell$ ) is omitted for notational simplicity. The inter-method wideband covariance matrix  $\mathbf{R}_{\mathbf{z}} \in \mathbb{C}^{2 \times 2}$  in (13) is then re-written as

$$\begin{aligned}
\mathbf{R}_z &= \mathbb{E}\{\mathbf{Z}\mathbf{Z}^H\} \\
&= \mathbb{E}\left\{\begin{bmatrix} \check{\mathbf{s}}\check{\mathbf{s}}^H & \check{\mathbf{s}}\check{\mathbf{s}}^H \\ \check{\mathbf{s}}\check{\mathbf{s}}^H & \check{\mathbf{s}}\check{\mathbf{s}}^H \end{bmatrix}\right\} + \mathbb{E}\left\{\begin{bmatrix} \check{\mathbf{n}}_{\text{Hyb}}\check{\mathbf{n}}_{\text{Hyb}}^H & \check{\mathbf{n}}_{\text{Hyb}}\check{\mathbf{n}}_{\text{Iso}}^H \\ \check{\mathbf{n}}_{\text{Iso}}\check{\mathbf{n}}_{\text{Hyb}}^H & \check{\mathbf{n}}_{\text{Iso}}\check{\mathbf{n}}_{\text{Iso}}^H \end{bmatrix}\right\} \\
&+ \mathbb{E}\left\{\begin{bmatrix} \check{\mathbf{n}}_{\text{Hyb}}\check{\mathbf{n}}_{\text{Hyb}}^H & \check{\mathbf{n}}_{\text{Hyb}}\check{\mathbf{n}}_{\text{Iso}}^H \\ \check{\mathbf{n}}_{\text{Iso}}\check{\mathbf{n}}_{\text{Hyb}}^H & \check{\mathbf{n}}_{\text{Iso}}\check{\mathbf{n}}_{\text{Iso}}^H \end{bmatrix}\right\} + \mathbb{E}\left\{\begin{bmatrix} \check{\mathbf{n}}_{\text{Hyb}}\check{\mathbf{s}}^H & \check{\mathbf{n}}_{\text{Hyb}}\check{\mathbf{s}}^H \\ \check{\mathbf{n}}_{\text{Iso}}\check{\mathbf{s}}^H & \check{\mathbf{n}}_{\text{Iso}}\check{\mathbf{s}}^H \end{bmatrix}\right\}.
\end{aligned} \quad (32)$$

Since  $\check{\mathbf{s}}$ ,  $\check{\mathbf{n}}_{\text{Iso}}$  and  $\check{\mathbf{n}}_{\text{Hyb}}$  are uncorrelated, (32) can be simplified to

$$\begin{aligned}
\mathbf{R}_z &= \|\check{\mathbf{s}}\|^2 \mathbf{J} + \begin{bmatrix} \|\check{\mathbf{n}}_{\text{Hyb}}\|^2 & 0 \\ 0 & \|\check{\mathbf{n}}_{\text{Iso}}\|^2 \end{bmatrix} \\
&= \|\check{\mathbf{s}}\|^2 \mathbf{j}\mathbf{j}^H + \sigma_1 \mathbf{I} + \sigma_2 \mathbf{K},
\end{aligned} \quad (33)$$

$$\text{where } \sigma_1 = \left(\frac{\|\check{\mathbf{n}}_{\text{Hyb}}\|^2 + \|\check{\mathbf{n}}_{\text{Iso}}\|^2}{2}\right), \quad (34)$$

$$\text{and } \sigma_2 = \left(\frac{\|\check{\mathbf{n}}_{\text{Hyb}}\|^2 - \|\check{\mathbf{n}}_{\text{Iso}}\|^2}{2}\right), \quad (35)$$

where  $\mathbf{J} = \mathbf{j}\mathbf{j}^H \in \mathbb{R}^{2 \times 2}$  is the all-one matrix with  $\mathbf{j} = [1, 1]^T$  being all-one column-vector,  $\mathbf{I} = \text{diag}([1, 1]) \in \mathbb{R}^{2 \times 2}$  is the identity matrix and  $\mathbf{K} = \text{diag}([1, -1]) \in \mathbb{R}^{2 \times 2}$  is the signature matrix. Hence, the signal subspace in the inter-method PCA is expected to dominantly include  $\check{\mathbf{s}}$  that is the most correlated component between the  $\check{\mathbf{z}}_{\text{Hyb}}$  and  $\check{\mathbf{z}}_{\text{Iso}}$  and avoids the least correlated component between the two that is the musical noise only present in  $\check{\mathbf{n}}_{\text{Hyb}}$ .

#### REFERENCES

- [1] E. C. Cherry, "Some experiments on the recognition of speech, with one and with two ears," *J. Acoust. Soc. Am.*, vol. 25, no. 5, pp. 975–979, Sep. 1953.
- [2] A. W. Bronkhorst, "The cocktail party phenomenon: A review of research on speech intelligibility in multiple-talker conditions," vol. 86, pp. 117–128, 2000.
- [3] J. Donley, V. Tourbabin, J.-S. Lee, M. Broyles, H. Jiang, J. Shen, M. Pantic, V. K. Ithapu, and R. Mehra, "Easy-Com: An Augmented Reality Dataset to Support Algorithms for Easy Communication in Noisy Environments," Oct. 2021.
- [4] "SPEAR challenge website," <https://imperialcollegelondon.github.io/spear-challenge>.
- [5] S. Doclo, S. Gannot, M. Moonen, and A. Spriet, "Acoustic beamforming for hearing aid applications," in *Handbook on Array Processing and Sensor Networks*, S. Haykin and K. J. R. Liu, Eds. John Wiley & Sons, Inc., 2010, pp. 269–302.
- [6] H. W. Löllmann, A. H. Moore, P. A. Naylor, B. Rafaely, R. Horaud, A. Mazel, and W. Kellermann, "Microphone array signal processing for robot audition," in *Proc. Joint Workshop on Hands-Free Speech Communication and Microphone Arrays (HSCMA)*, San Francisco, CA, USA, Mar. 2017, pp. 51–55.
- [7] T. J. Klaseen, T. Van den Bogaert, M. Moonen, and J. Wouters, "Binaural noise reduction algorithms for hearing aids that preserve interaural time delay cues," *IEEE Trans. Signal Process.*, vol. 55, no. 4, pp. 1579–1585, Apr. 2007.
- [8] R. Haeb-Umbach, S. Watanabe, T. Nakatani, M. Bacchiani, B. Hoffmeister, M. L. Seltzer, H. Zen, and M. Souden, "Speech processing for digital home assistants: Combining signal processing with deep-learning techniques," *IEEE Signal Processing Magazine*, vol. 36, no. 6, pp. 111–124, Nov 2019.
- [9] J. Benesty, M. M. Sondhi, and Y. Huang, Eds., *Springer Handbook of Speech Processing*, 1st ed. Springer-Verlag, 2008.
- [10] N. Wiener, *The Extrapolation, Interpolation and Smoothing of Stationary Time Series*. New York, NY, USA: John Wiley & Sons, Inc., 1949.
- [11] P. Loizou, *Speech Enhancement: Theory and Practice*. Boca Raton, USA: CRC Press, 2007.
- [12] Y. Hu, Y. Liu, S. Lv, M. Xing, S. Zhang, Y. Fu, J. Wu, B. Zhang, and L. Xie, "DCCRN: Deep Complex Convolution Recurrent Network for Phase-Aware Speech Enhancement," in *Interspeech 2020*, Oct. 2020, pp. 2472–2476.
- [13] Y. Luo and N. Mesgarani, "TasNet: Time-domain audio separation network for real-time, single-channel speech separation," Apr. 2018.
- [14] S. Hafezi, A. H. Moore, P. Guiraud, P. A. Naylor, J. Donley, V. Tourbabin, and T. Lunner, "Subspace hybrid beamforming for head-worn microphone arrays," in *Proc. IEEE Int. Conf. on Acoust., Speech and Signal Process. (ICASSP)*, 2023, pp. 1–5.
- [15] S. Gannot, E. Vincent, S. Markovich-Golan, and A. Ozerov, "A consolidated perspective on multimicrophone speech enhancement and source separation," *IEEE/ACM Trans. Audio, Speech, Language Process.*, vol. 25, no. 4, pp. 692–730, Apr. 2017.
- [16] D. E. Dudgeon and R. M. Mersereau, *Multidimensional Digital Signal Processing*, 1984.
- [17] J. Capon, "High-resolution frequency-wavenumber spectrum analysis," *Proc. IEEE*, vol. 57, no. 8, pp. 1408–1418, Aug. 1969.
- [18] H. L. van Trees, *Optimum Array Processing*, ser. Detection, Estimation and Modulation Theory. John Wiley & Sons, Inc., 2002.
- [19] —, "Optimum waveform estimation," in *Optimum Array Processing*. New York, USA: John Wiley & Sons, Inc., Apr. 2002, vol. IV, Optimum Array Processing, ch. 6, pp. 428–709.
- [20] H. Cox, "Resolving power and sensitivity to mismatch of optimum array processors," *J. Acoust. Soc. Am.*, vol. 54, no. 3, pp. 771–785, Sep. 1973.
- [21] L. Ehrenberg, S. Gannot, A. Leshem, and E. Zehavi, "Sensitivity analysis of MVDR and MPDR beamformers," in *IEEE Conv. Electrical and Electronics Engineers*, Eilat, Israel, Nov. 2010, pp. 416–420.
- [22] E. E. Jan and J. Flanagan, "Sound capture from spatial volumes: Matched-filter processing of microphone arrays having randomly-distributed sensors," in *Proc. IEEE Int. Conf. on Acoust., Speech and Signal Process. (ICASSP)*, Atlanta, Georgia, USA, May 1996, pp. 917–920.
- [23] J. Bitzer and K. U. Simmer, "Superdirective microphone arrays," in *Microphone Arrays: Signal Processing Tech-*

- niques and Applications*, ser. Digital Signal Processing, M. Brandstein and D. Ward, Eds. Berlin, Heidelberg: Springer, 2001, pp. 19–38.
- [24] A. H. Moore, S. Hafezi, R. R. Vos, P. A. Naylor, and M. Brookes, “A Compact Noise Covariance Matrix Model for MVDR Beamforming,” *IEEE/ACM Transactions on Audio, Speech, and Language Processing*, vol. 30, pp. 2049–2061, 2022.
- [25] A. Pandey, B. Xu, A. Kumar, J. Donley, P. Calamia, and D. Wang, “TPARN: Triple-path attentive recurrent network for time-domain multichannel speech enhancement,” in *Proc. IEEE Int. Conf. on Acoust., Speech and Signal Process. (ICASSP)*, 2022, pp. 6497–6501.
- [26] J. Casebeer, J. Donley, D. Wong, B. Xu, and A. Kumar, “Nice-beam: Neural integrated covariance estimators for time-varying beamformers,” 2021.
- [27] J. Heymann, L. Drude, and R. Haeb-Umbach, “Neural network based spectral mask estimation for acoustic beamforming,” in *2016 IEEE International Conference on Acoustics, Speech and Signal Processing (ICASSP)*, Mar. 2016, pp. 196–200.
- [28] Z.-Q. Wang and D. Wang, “All-Neural Multi-Channel Speech Enhancement,” in *Proc. Interspeech 2018*, Sep. 2018, p. 3238.
- [29] D. Wang and C. Bao, “Multi-channel Speech Enhancement Based on the MVDR Beamformer and Postfilter,” in *2020 IEEE International Conference on Signal Processing, Communications and Computing (ICSPCC)*, Aug. 2020, pp. 1–5.
- [30] Z. Zhang, Y. Xu, M. Yu, S.-X. Zhang, L. Chen, and D. Yu, “ADL-MVDR: All Deep Learning MVDR Beamformer for Target Speech Separation,” in *ICASSP 2021 - 2021 IEEE International Conference on Acoustics, Speech and Signal Processing (ICASSP)*, Jun. 2021, pp. 6089–6093.
- [31] Y. Liu, A. Ganguly, K. Kamath, and T. Kristjansson, “Neural network based time-frequency masking and steering vector estimation for two-channel mvdr beamforming,” in *IEEE International Conference on Acoustics, Speech and Signal Processing (ICASSP)*. IEEE, Apr 2018.
- [32] H. Erdogan, J. R. Hershey, S. Watanabe, M. I. Mandel, and J. Le Roux, “Improved MVDR beamforming using single-channel mask prediction networks,” in *Proc. Interspeech*, 2016, pp. 1981–1985.
- [33] X. Ren, X. Zhang, L. Chen, X. Zheng, C. Zhang, L. Guo, and B. Yu, “A Causal U-Net Based Neural Beamforming Network for Real-Time Multi-Channel Speech Enhancement,” in *Interspeech 2021*, Aug. 2021, pp. 1832–1836.
- [34] Y. Chen, Y. Hsu, and M. R. Bai, “Multi-channel end-to-end neural network for speech enhancement, source localization, and voice activity detection,” Jun. 2022.
- [35] Y. Luo, C. Han, N. Mesgarani, E. Ceolini, and S.-C. Liu, “FaSNet: Low-Latency Adaptive Beamforming for Multi-Microphone Audio Processing,” in *2019 IEEE Automatic Speech Recognition and Understanding Workshop (ASRU)*, Dec. 2019, pp. 260–267.
- [36] H. Cox, R. M. Zeskind, and M. M. Owen, “Robust adaptive beamforming,” *IEEE Trans. Signal Process.*, vol. 35, no. 10, pp. 1365–1376, Oct. 1987.
- [37] J. Li, P. Stoica, and Z. Wang, “On robust capon beamforming and diagonal loading,” *IEEE Trans. Signal Process.*, vol. 51, no. 7, pp. 1702–1715, Jul. 2003.
- [38] J. R. Driscoll and D. M. Healy, “Computing Fourier transforms and convolutions on the 2-sphere,” *Advances in Applied Mathematics*, vol. 15, no. 2, pp. 202–250, Jun. 1994.
- [39] mh acoustics, “EM32 Eigenmike microphone array release notes (v17.0),” M. H. Acoust., NJ USA, Hardware, Oct. 2013. [Online]. Available: <http://www.mhacoustics.com/sites/default/files/ReleaseNotes.pdf>
- [40] G. Grimm, J. Luberadzka, and V. Hohmann, “A toolbox for rendering virtual acoustic environments in the context of audiology,” *Acta Acustica united with Acustica*, vol. 105, no. 3, pp. 566–578, 2019.
- [41] C. H. Taal, R. C. Hendriks, R. Heusdens, and J. Jensen, “An algorithm for intelligibility prediction of time-frequency weighted noisy speech,” *IEEE Trans. Audio, Speech, Language Process.*, vol. 19, no. 7, pp. 2125–2136, Sep. 2011.
- [42] ITU-T, “Perceptual evaluation of speech quality (PESQ), an objective method for end-to-end speech quality assessment of narrowband telephone networks and speech codecs,” Int. Telecommun. Union (ITU-T), Recommendation P.862, Nov. 2003.
- [43] A. Rix, J. Beerends, M. Hollier, and A. Hekstra, “Perceptual evaluation of speech quality (PESQ)-a new method for speech quality assessment of telephone networks and codecs,” in *Proc. IEEE Int. Conf. on Acoust., Speech and Signal Process. (ICASSP)*, vol. 2, Salt Lake City, UT, USA, May 2001, pp. 749–752.
- [44] J. Tribolet, P. Noll, B. McDermott, and R. Crochiere, “A study of complexity and quality of speech waveform coders,” in *Proc. IEEE Int. Conf. on Acoust., Speech and Signal Process. (ICASSP)*, vol. 3, Tulsa, OK, USA, Apr. 1978, pp. 586–590.
- [45] Y. Hu and P. C. Loizou, “Evaluation of objective quality measures for speech enhancement,” *IEEE Trans. Audio, Speech, Language Process.*, vol. 16, no. 1, pp. 229–238, Jan. 2008.
- [46] E. Vincent, R. Gribonval, and C. Févotte, “Performance measurement in blind audio source separation,” *IEEE Trans. Audio, Speech, Language Process.*, vol. 14, no. 4, pp. 1462–1469, Jul. 2006.
- [47] D. M. Brookes, “VOICEBOX: A speech processing toolbox for MATLAB,” 1997. [Online]. Available: <http://www.ee.ic.ac.uk/hp/staff/dmb/voicebox/voicebox.html>
- [48] V. Emiya, E. Vincent, N. Harlander, and V. Hohmann, “Subjective and objective quality assessment of audio source separation,” *IEEE Transactions on Audio, Speech, and Language Processing*, vol. 19, no. 7, pp. 2046–2057, 2011.
- [49] E. Vincent, “PEASS: Perceptual evaluation methods for audio source separation toolbox for MATLAB,” 2017.
- [50] “SS-Hybrid audio demo [online],” <https://imperialcollegelondon.github.io/sap-SSHybrid-journal/>



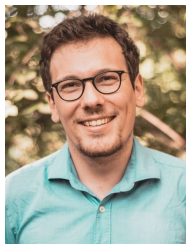
**Sina Hafezi** is a post-doctoral Research Associate at Imperial College London. He received the BEng degree in Electronic Engineering in 2012 and the MSc degree in Digital Signal Processing in 2013 both from Queen Mary, University of London, UK. He worked in the Centre for Digital Music as a researcher and software engineer on autonomous multitrack mixing systems, which led to patent and spin-out company. In 2018, he received his PhD in acoustic source localisation using spherical microphone arrays at Imperial College London, UK. He

spent 2.5 years at Silixa as Senior Signal Processing Engineer developing algorithms and software for Distributed Acoustic Sensing systems. In 2021, he re-joined Imperial College London, where he has contributed to academic and industrial projects on hearing aids and spatial audio. His research interests are microphone array processing, spatial audio rendering, beamforming, source localisation and room acoustic modelling with applications for augmented and virtual reality.



**Alastair H. Moore** (M'13) is a Research Fellow at Imperial College London and spatial audio consultant with Square Set Sound. He received the M.Eng. degree in Electronic Engineering with Music Technology Systems in 2005 and the Ph.D. degree in 2010, both from the University of York, York, U.K. He spent 3 years as a Hardware Design Engineer for Imagination Technologies PLC designing digital radios and networked audio consumer electronics products. In 2012, he joined Imperial College, where he has contributed to a series of projects in the field

of speech and audio processing applied to voice over IP, robot audition, and hearing aids. Particular topics of interest include microphone array signal processing, modeling and characterization of room acoustics, dereverberation, and spatial audio perception. His current research is focused on signal processing for moving, head-worn microphone arrays.



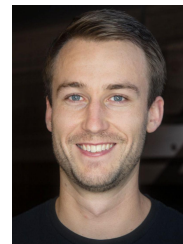
**Pierre H. Guiraud** is a post-doctoral Research Associate at Imperial College London. After enrolling in a double degree program, he received a MSc in Engineering from the Ecole Centrale de Lille, France, as well as a Master in Engineer Acoustic from the Technical University of Denmark in Copenhagen in 2017. His master thesis focused on ambisonic sound reproduction in collaboration with the company Kahle Acoustics. He went on to pursue a PhD at the IEMN in Lille, France, about thermoacoustic sound generation in porous

metamaterials. This work was sponsored by Thales Underwater Systems and done in partnership with CINTRA Singapore. He obtained his PhD in 2020 and joined Imperial College London in 2021 working on several projects. Within the Speech and Audio Processing group, he worked on the SPEAR Challenge which is an IEEE challenge about speech enhancement for Virtual/Augmented Reality in partnership with Meta Reality Labs Research. Within the ELO-SPHERES project, he worked on how to improve binaural intelligibility metrics in real environments using deep learning, in collaboration with University College London. Lastly, in the Audio Experience Design research group, he was in charge of an experiment on spatial audioperception in a virtual reality environment.



**Patrick A. Naylor** (M'89, SM'07, F'20) is Professor of Speech and Acoustic Signal Processing at Imperial College London. He received the BEng degree in Electronic and Electrical Engineering from the University of Sheffield, UK, and the PhD degree from Imperial College London, UK. His research interests are in speech, audio and acoustic signal processing. His current research addresses microphone array signal processing, speaker diarization, and multichannel speech enhancement for application to binaural hearing aids and robot audition. He has

also worked on speech dereverberation including blind multichannel system identification and equalization, acoustic echo control, non-intrusive speech quality estimation, and speech production modelling with a focus on the analysis of the voice source signal. In addition to his academic research, he enjoys several collaborative links with industry. He is currently a member of the Board of Governors of the IEEE Signal Processing Society and President of the European Association for Signal Processing (EURASIP). He was formerly Chair of the IEEE Signal Processing Society Technical Committee on Audio and Acoustic Signal Processing. He has served as an associate editor of IEEE Signal Processing Letters and is currently a Senior Area Editor of IEEE Transactions on Audio Speech and Language Processing.



**Jacob Donley** is a research scientist at Meta Reality Labs Research in Redmond, WA with previous experience lecturing in Signals and Systems at the University of Wollongong (UOW) and Engineering at Western Sydney University. He holds a Bachelor of Engineering Honours (Computer) (UOW), a Ph.D. (UOW) with research focused on Digital Signal Processing (DSP) aimed at improving the reproduction of personal sound in shared environments, and a graduate certificate in Artificial Intelligence (AI) from Stanford University. Jacob's research interests

are in signal processing, speech enhancement, machine learning, array processing (microphone and loudspeaker), beamforming, and multi-zone sound field reproduction. Jacob has received awards and scholarships from Telstra Corporation Limited, the Australian Department of Education and Training, and the University of Wollongong. He is also an active member of the IEEE and IEEE Signal Processing Society.



**Vladimir Tourbabin** (M'16) is a Research Science Manager at Meta. He received the B.Sc. degree (summa cum laude) in materials science and engineering in 2005, the M.Sc. degree (cum laude) in electrical and computer engineering in 2011, and the PhD degree in electrical and computer engineering in 2016. All three degrees are from Ben-Gurion University of the Negev, Israel. After the graduation, he has joined the General Motors' Advanced Technical Center in Israel, to work on microphone array processing solutions for speech recognition. Since

2017, Dr. Tourbabin is with Reality Labs Research @ Meta (formerly known as Facebook Reality Labs) working on research and advanced development of audio signal processing technologies for augmented and virtual reality applications.



**Thomas Lunner's** career has focused on man-machine issues related to the correlation between hearing and cognition. He was the first scientist to convincingly show the importance of cognitive ability in relation to being able to recognize speech in adverse listening conditions. He also demonstrated how working memory was a significant factor for the selection of optimum signal processing in hearing aids to be fitted to a particular individual. These studies led to increasing cooperation with other research groups globally, and the establishment of cognitive hearing science as a research field of its own. Dr. Lunner's Ph.D. research in the mid-1990s resulted in patented signal processing algorithms which led to the development of the first digital hearing aid manufactured by Oticon. The core of this project was a digital filter bank which provided the necessary tuning flexibility with an equally important low power consumption. The filter bank was used in several successive hearing aid models in the years that followed, fitted to millions of hearing aid users worldwide. Two of the models were awarded the European Union's prestigious technology prize, the IST Grand Prize in 1996 and in 2003. Currently, he leads research in Superhuman Hearing at Meta Reality Labs Research.